Numerical simulation of a high responsivity ultraviolet photodetector

Fayçal Bouzid[1✉], Lakhdar Dehimi[2,3], Moufdi Hadjab[1], Abderrahim Hadj Larbi[1], Ammar Haboussi[1]

[1]*Research Center in Industrial Technologies CRTI, P.O. Box 64, Cheraga 16014, Algiers, ALGERIA.*

[2]*Batna University, Physics Department, Batna-ALGERIA.*

[3]*Laboratory of Metallic and Semiconductor Materials, University of Biskra, P.B.145, Biskra-ALGERIA.*

✉Corresponding Author Email: f.bouzid@crti.dz

Abstract

Ultraviolet photodetectors (UV PDs) are important devices that can be used in various scientific, commercial and military applications. In this work, a numerical simulation study of nitride-based "p^+-n-n^+" front illuminated UV PD, designed with an aluminum composition achieving a true solar blindness, has been reported using the commercially available Atlas package from Silvaco international. It has been found that the proposed structure is sensitive to the UV rays in the wavelength range investigated, where the spectral response reaches its maximum then declines sharply with a good performance of solar-blind at room temperature and zero-bias voltage. Furthermore, it was also found by simulating the evolution of the current density according to different wavelengths of the incident radiation that the designed structure is able to act as a wavelength selector device.

Keywords: *AlGaN, Ultraviolet, Solar blind, Photodetector, Spectral response.*

1. Introduction

Semiconductor-based radiation detectors have been developing for several years, with the advent of new detection methods and materials, applications in various fields which extend to material science, astrophysics, industrial and medical sectors, as well as control and the environment. Gallium Nitride (GaN) is one of the most interesting semiconductor compounds, well suited to work in any application in which the temperature or level of radiation could damage conventional silicon (Si) or gallium arsenide (GaAs) electronics [1]. Compared with other materials, the most attractive properties of GaN are: a wide bandgap (3.4 eV), high saturation velocity, high thermal conductivity, strong electrical breakdown field, and an ability to form high quality heterostructures with good transport properties [2]. In recent years, a large number of GaN-based devices have been developed, such as light-emitting diodes, laser diodes, photodetectors and particle detectors [3-7].
Recently, AlGaN-based "p^+-n-n^+" UV photodetectors have received a lot of attention [8-10]. In most of these photodetectors, the light must pass through a "window" layer before reaching the absorbing layer (n-region). These photodetectors often operate under a low reverse bias with a relatively constant electric field across the entire n-AlGaN layer where a space charge region is formed [11].
In this work, we have designed a high responsivity "p^+-n-n^+" UV-light detector based on the $Al_xGa_{1-x}N$ ternary compound for frontal lighting, where the aluminum molar fraction chosen for our design is equal to 0.17, by means of SILVACO-Atlas computer-aided design software (TCAD) [12], considering a two-dimensional (2D) analysis, solving the Poisson equation and the equations of continuities of the charge carriers. The chosen aluminum molar fraction corresponds to a cut-off wavelength equal to 0.31 μm, which guarantees a true solar blindness. The effect of the radiation wavelength, temperature as well as the applied reverse-bias voltage on the spectral response were also evaluated.

2. Structure description

The materials used in our device are $Al_xGa_{1-x}N$ with $x = 0.17$ and GaN, with electrodes on the top and bottom of the device which are both ohmic contacts, where the metal used for the anode is platinum (Pt) with a thickness equal to 5 nm and a length equal to 2.9 microns, while the cathode is an Al / Si / Cu multilayer over the entire rear surface of the detector. The total detector area is 12 μm^2. The schema of the proposed structure is shown in Fig. (1):

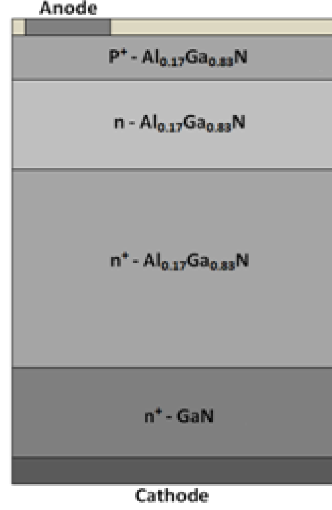

Fig. 1: Schematic of the studied photodetector structure.

As can be seen in Fig. (1), below the anode we have an $Al_{0.17}Ga_{0.83}N$ epitaxial layer of 0.1 µm thickness doped "p^+" with a concentration of acceptors equal to 1.0×10^{16} cm^{-3}. The intrinsic region is a 0.2 µm $Al_{0.17}Ga_{0.83}N$ layer doped "n" at 1.0×10^{13} cm^{-3}.

The main disadvantage of the "p^+-n-n^+" detectors based on the AlGaN compound is the difficulty of forming high quality ohmic contacts on AlGaN layers. To overcome this problem, researchers often use a thin layer of highly doped GaN below the "n^+" region to be in contact with the metal. Therefore, in our low ohmic contact design we used a 0.8 µm n^+-$Al_{0.17}Ga_{0.83}N$ layer doped at 5.0×10^{17} cm^{-3} and a 0.2 µm n^+-GaN layer with a doping concentration of 8.0×10^{19} cm^{-3}.

The total current density depends mainly on the generation-recombination phenomenon that occurs within the active region. Therefore, in this active region and in the vicinity of the interface between two different doping regions, the calculation must be precise in order to allow the convergence of the simulation. For this reason, in the "p^+" epitaxial layer and at the interface with the "n" type layer as well as the interface between the "n" layer and the "n^+" layer, the mesh is tighter. On the contrary, in the "n^+" type layers, the mesh is relaxed.

3. Results and discussion

3. 1 Analysis of the reverse-bias voltage effect on the spectral response

In order to know how the spectral response of our detector behaves when changing the applied reverse voltage at $T = 300$ K and by fixing the intensity of the light at 1.0 Wcm^{-2}, we simulated this response for different reverse voltages. The obtained results are shown in Fig. (2).

The peak of the spectral response results in 0.156 AW^{-1} for $\lambda = 0.29$ µm and at a zero-bias voltage, as shown in Fig. (2). This value increases to 0.16 AW^{-1} for a reverse bias voltage of -50 V. The observed increase in spectral response with the increase of the applied reverse bias should be related to the improvement of the charge collection efficiency.

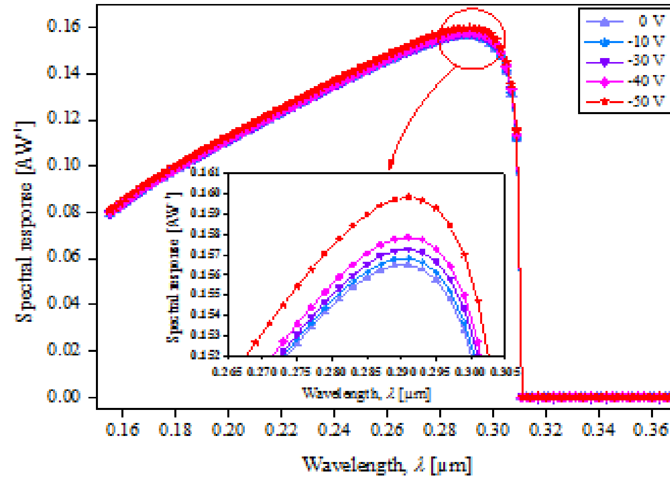

Fig. 2: Spectral response of the detector for different reverse bias voltages at $T = 300$ K and a light intensity of 1.0 Wcm^{-2}. The inset shows a zoom-in view of the spectral response from 0.265 µm to 0.305 µm.

3. 2 Analysis of the temperature effect on the spectral response

By illuminating the device in the wavelength range 0.155 µm - 0.37 µm, with a luminous intensity of 1.0 Wcm^{-2}, the curves obtained from the spectral response as a function of temperature are shown in Fig. 3.

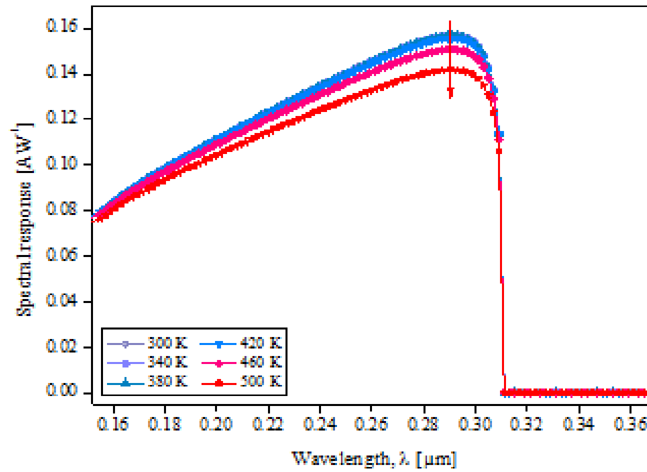

Fig. 3: Spectral response of the detector under a luminous intensity of 1.0 Wcm^{-2} and zero bias voltage, at six different temperatures.

From Fig. (3) above, it can be seen that the spectral response increases gradually from 0.079 AW^{-1} at the wavelength 0.155 µm to 0.156 AW^{-1} at 0.29 µm ($T = 300$ K) because of the increase in penetration depth, then it drops sharply at 0.31 µm (cut-off wavelength). In addition, we can note that the temperature effect on the spectral response for short wavelengths is limited because most of the corresponding photons are absorbed. It is also noted that the increase of the temperature from 300 K to 500 K causes a decrease in the spectral response so that the peak of the response at $T = 500$ K is 0.141 AW^{-1}. This decrease will be remarkable only when the temperature exceeds 420 K. This result is well explained by the thermal agitation of the crystal lattice which becomes more intense when the temperature increases, resulting in a reduction of the minority carriers mobility, lifetimes and diffusion coefficients. As a result, the recombination mechanism becomes stronger and dominates the photogeneration phenomena, which induces a reduction of the spectral response.

3. 3 Effect of the incident radiation wavelength on the *J*(*V*) characteristics

The evolution of the current density as a function of different wavelengths of the incident radiation is simulated, by using the optimized parameters of the p^{+}-region, and shown in Fig. (4).

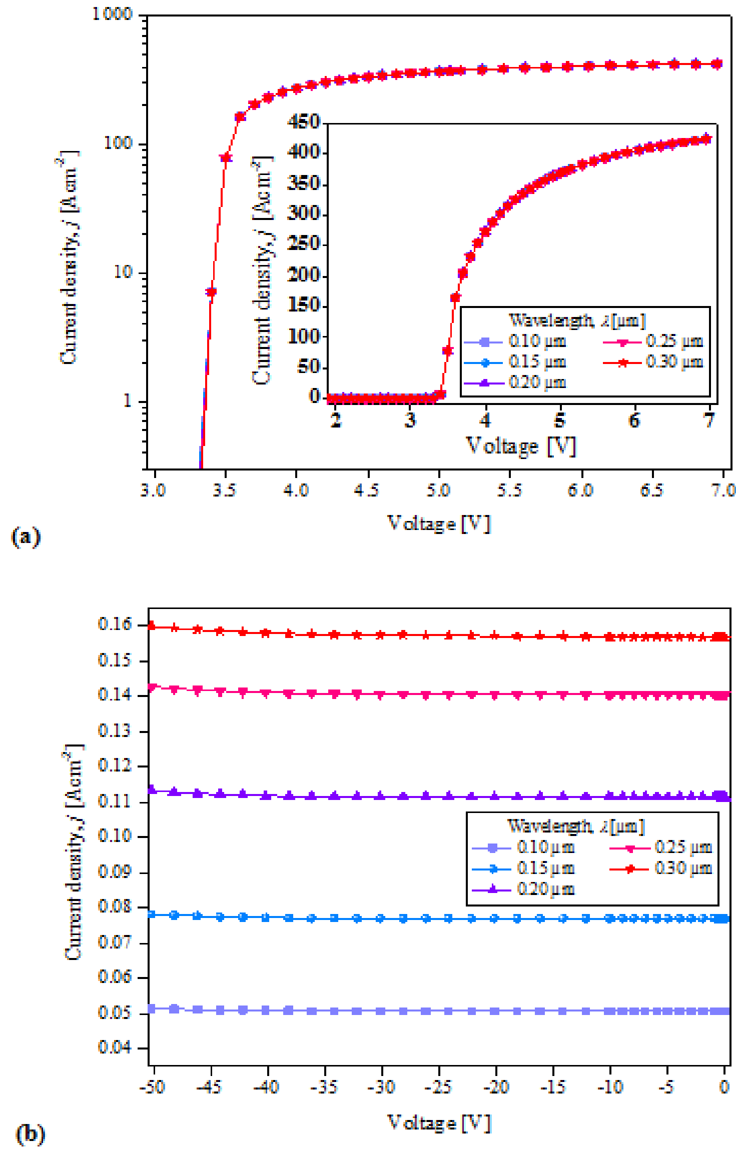

Fig. 4: *J*(*V*) characteristic for different wavelengths of incident radiation at $T = 300$ K and under a luminous intensity of 1.0 Wcm^{-2}. (a) Forward bias, (b) Reverse bias.

We note that the current density for direct-bias voltages remains unchanged. However, it is different for each wavelength under reverse-bias voltages. This increase in the reverse current is due to the improvement of the photogeneration rate as shown in Fig. (5).

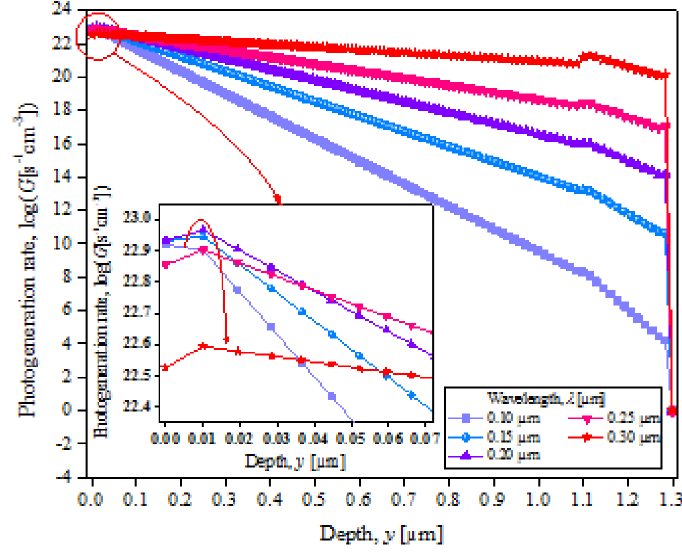

Fig. 5: Photogeneration rate profile across the detector for different wavelengths of incident radiation at $T = 300$ K and under a luminous intensity of 1.0 Wcm^{-2}.

In the encircled region of Fig. (5), it is found that the photogeneration rate decreases slightly near the detector surface with the increase of the incident radiation wavelength, while the opposite occurs in the volume of the detector. This phenomenon is mainly due to the large penetration depth of long wavelengths in the device volume, in contrast to the low wavelengths that are well absorbed at low thicknesses. These results clearly show that our UV photodetector capable of acting as a light wavelengths selector device.

4. Conclusion

The evaluation of the performances of the designed AlGaN-based "p^+-n-n^+" photodetector showed that this structure is sensitive to the UV rays of different wavelengths.
It was found that increasing the temperature from 300 K to 500 K causes a decrease in the spectral response when the temperature exceeds 420 K. Furthermore, the studied structure ensures a spectral response exceeding 0.15 AW^{-1} at room temperature and under zero-bias voltage.
On the other hand, the simulation of the $J(V)$ characteristics under UV lightning has shown that this radiation has no appreciable effect on the direct current density. While, the reverse current presents a different order of magnitude for each wavelength, so that the shorter wavelength generates the greatest leakage current.

References

[1] G. Wang, K. Fu, C. S. Yao, D. Su, G. G. Zhang, J. Y. Wang, and M. Lu, Nucl. Instrum. Methods Phys. Res., Sect. A 663, 10 (2012).
[2] M. S. P. Reddy, A. A. Kumar, and V. R. Reddy, Thin Solid Films 519, 3844 (2011).
[3] F. Bouzid, L. Dehimi, and F. Pezzimenti, Journal of Elec Materi 46, 6563 (2017).
[4] F. Bouzid, F. Pezzimenti, L. Dehimi, M. L. Megherbi, and F. G. Della Corte, Jpn. J. Appl. Phys. 56, 094301(2017).
[5] L. C. Chen, C. Y. Hsu, W. H. Lan, and S. Y. Teng, Solid-State Electron. 47, 1843 (2003).
[6] Y. K. Su, F. S. Juang, and M. H. Chen, Jpn. J. Appl. Phys. 42, 2257 (2003).
[7] R. Werner, M. Reinhardt, M. Emmerling, A. Forchel, V. Harle, and A. Bazhenov, Physica E 7, 915 (2000).
[8] N. Biyikli, and I. Kimukin, IEEE Photonics Technology Letters 16, no. 7, 1718 (2004).
[9] O. Ambacher, B. Foutz, and J. Smart, J. Appl. Phys., vol. 87, 334 (2000).

[10] Parish, G., Keller, S., Kozodoy, P., Ibbetson, J.P., Marchand, H., Fini, P.T., Fleischer, S.B., Den Baars, S.P., Mishra, U.K., Tarsa, E.J., Appl. Phys. Lett. 75, 247 (1999).
[11] Zetian Mi, Chennupati Jagadish, *III-Nitride Semiconductor Optoelectronics*, Volume 96 (*Semiconductors and Semimetals*) 1st Edition, Volume 96, Elsevier Inc., 2017.
[12] Silvaco Atlas User's Manual, Device Simulator Software (2013).